A Near-Ultraviolet Spectroscopic Survey of B-Type Asteroids

by

Ashley J. Peter

Submitted to the Department of Earth, Atmospheric and Planetary Sciences

in Partial Fulfillment of the Requirements for the Degree of

Bachelor of Science in Earth, Atmospheric and Planetary Sciences

at the Massachusetts Institute of Technology

May 13, 2015 [June 2015]

Author Signature redacted

Department of Earth, Atmospheric and Planetary Sciences

May 13, 2015

Certified by Signature redacted

Richard P. Binzel

Thesis Supervisor

Accepted by Signature redacted

Richard P. Binzel

Chair, Committee on Undergraduate Program

A Near-Ultraviolet Spectroscopic Survey of B-Type Asteroids

Ashley J. Peter

Advisors

Julia de León, PhD
Instituto de Astrofísica de Canarias, Universidad de La Laguna

Javier Licandro, PhD
Instituto de Astrofísica de Canarias

Richard P. Binzel, PhD
Massachusetts Institute of Technology

Abstract

This study aimed to evaluate the presence of spectral slope variations of B-type asteroids in the near-ultraviolet wavelength range and further compare variations to those found in the near-infrared (de León et al., 2012) and infrared (Alí-Lagoa et al., 2013). New observations of 19 B-type asteroids were obtained using the Telescopio Nazionale Galileo (TNG) and additional observations were collected on the William Herschel Telescope (WHT) and Isaac Newton Telescope (INT). After identifying appropriate solar analogs for spectral reduction, it was found that 1) not all asteroids are B-types as classified by the M4AST online tool (Popescu et al., 2012), and 2) spectral slope variations were present amongst the B-type asteroids. These spectral slope variations could not be traced to the use of certain solar analogs or differences in airmass during observations. Furthermore, these variations were in good agreement spectral slope variations of carbonaceous chondrites, particularly in the near-UV region. These results support the work of de León et al. (2012) and Alí-Lagoa et al. (2013) in identifying spectral slope variations and contributing to a three-part survey of B-type asteroids across different wavelengths.

Acknowledgements

I would like to thank Julia de León for her constant patience and guidance throughout this process. Without her, this work would not have been possible. I would also like to thank Javier Licandro for giving me the opportunity to work with him at the Instituto de Astrofísica de Canarias for one summer and helping me through throughout this process. My trip to the Canary Islands would not have been possible without the funding of the MIT International Science and Technology Initiatives (MISTI) program and International Research Opportunity Program (IROP).

I would also like to thank Professor Richard Binzel for his support and guidance over the past four years. He has been an incredible mentor and advisor throughout my college career.

Lastly, I would like to thank my parents for always encouraging me to pursue my goals and supporting me in whatever I do.

Contents

1 Introduction

Observations of asteroids are fundamental to our understanding of planet formation and the existence of life on Earth. In our solar system today, asteroids are direct remnants of the original building blocks that formed the planets. Therefore, asteroids contain a good record of the initial conditions of our solar nebula 4.6 billion years ago. The asteroids that have survived have experienced collisional, dynamical, and thermal events that have shaped their present-day physical and orbital properties. Studying these asteroids gives us insight about how the bodies in our solar system have evolved (Bottke et al., 2003).

This study focuses on a rare subset of carbon-rich asteroids, referred to as B-type asteroids, which can be found in the middle and outer main asteroid belt of our solar system. These primitive, low-albedo, and volatile-rich asteroids are classified by their visible spectra, which are linear and featureless in the 5500-9000 Å wavelength range. B-type asteroids are named for the color of their spectral slope: through observations, it has been noted that they exhibit a negative (blue) spectral slope from ~0.5 to ~1.1 μm (Clark et al., 2010; de León, 2012).

B-type asteroids have been shown to be linked very closely to carbonaceous chondrites, or specific types of carbon-rich meteorites (Licandro et al., 2007; de León et al., 2012; Clark et al., 2010; Vilas and Gaffey, 1989; Vilas et al., 1994). Since we have samples of these meteorites in our physical possession, we have a better understanding of their features and compositions than we would by inferring from observations of their potential parent asteroids in space. It is believed that carbonaceous chondrites and their possible parent analogs – carbonaceous asteroids – chemically match the primordial composition of the early solar system, with only the lighter elements and volatiles removed (Weigert et al., 2007). Since B-type asteroids are closely linked to carbonaceous chondrites, it is therefore suggested that B-types also represent the primordial chemical composition of the early solar system.

A comprehensive study by Clark et al. (2010) examined the spectral properties of B-type asteroids in the near-infrared (0.8-2.5 μm) and further divided them into three categories: 1) those that resemble asteroid 2 Pallas; 2) those that resemble asteroid 24 Themis; 3) those that do not fall into either category.

Although these three groups help define the larger B-type population, variations still exist within the categories. Previous studies indicate that the spectral slopes of B-type asteroids are non-constant and instead exhibit variations. Johnson and Fanale (1973) studied a sample of carbonaceous chondrites that closely resemble B-type asteroids in their compositions. Results suggest that spectral variations are linked to grain size; and furthermore that bluer spectra are indicative of larger grain sizes. In addition, Johnson and Fanale found that carbon and magnetite seem to contribute to the overall blue slope of these asteroids specifically in the visible and near-infrared regions. Although we have an understanding of the spectral properties of B-type asteroids, we still do not understand the causes of slope variations in different wavelength regions.

In order to further understand B-type spectral variations across wavelengths, this study will contribute to a three-part spectroscopic survey of B-type asteroids conducted by de León et al. (2012) in the near-infrared region and Alí-Lagoa et al. (2013) in the infrared range in order to gain a more comprehensive understanding of their spectra. Contrary to the three clearly defined groups of Clark et al. (2010), de León et al. (2012) analyzed 45 B-type asteroids in the near-infrared and found a continuous shape variation in their reflectance spectra, ranging from a monotonic negative (blue) slope to a positive (red) slope. This continuous spectral trend fills the gap in the separation between the two main groups defined by Clark et al. in 2010. Furthermore, after clustering the asteroid spectra into six "centroids," the study found that the best meteorite analogs for the six clusters were carbonaceous chondrites that gradually changed in their degrees of hydration. Alí-Lagoa et al. (2013) found a similar behavior after analyzing B-type asteroids from NASA's Wide-field Infrared Explorer (WISE) observations in the infrared. Results further confirmed that the gradual variations in spectral slope found by de León et al. could be linked to the presence of water.

This study will contribute to the work of de León et al. and Alí-Lagoa et al. by extending spectral observations and analysis of B-type asteroids to the near-ultraviolet range from 0.3-0.8 μm. It aims to search for similar spectral variability in this wavelength region to provide a more comprehensive understanding of the behavior of B-type asteroids. Previous surveys, such as the Small Main-Belt Asteroid Spectroscopic Survey (SMASS, Bus and Binzel, 2002) show spectral variations in B-types shortwards of 0.55 μm, but the wavelength coverage does not extend below 0.43 μm. The near-UV spectral region between 0.3 and 0.5 μm often contains a changing spectral slope and thus can be very

diagnostic of the composition of B-types. Therefore, it is important to analyze this region in great detail. The Eight Color Asteroid Survey (ECAS, Zellner et al., 2009) does include data in this region, but unfortunately with low spectral resolution and for few B-type objects. Our survey, however, extends from 0.3 to 0.8 μm (including the important near-UV region) and aims to search for similar spectral variability found by de León et al. (2012) and Alí-Lagoa et al. (2013) in order to better understand B-types as a whole.

A complementary goal of this study is to investigate the effectiveness of solar analogs in reducing asteroid spectra. Solar analog stars are integral to spectroscopic observations in removing the solar continuum from the asteroid continuum. Observers generally select solar analogs from the Landolt catalog (Landolt, 1992) based on the stars' proximities to the object being observed ensuring similar airmass. These solar analogs have been proven to behave like the Sun in the visible to near-infrared wavelength range. However, most of them have not been tested in the near-ultraviolet wavelengths and can cause inaccurate subtraction of solar reflectances or variations in spectral slope. This study analyzes the behaviors of different solar analogs in Section 3.1 and determines which are the most suitable for spectral observations of asteroids.

2 Observations

New observations of 19 B-type asteroids were conducted on the nights of February 6, 7, and 8 in 2012. Low resolution, near-ultraviolet spectra were taken with the 3.58-m Telescopio Nazionale Galileo (TNG) located at the El Roque de Los Muchachos Observatory, in La Palma (Canary Islands), Spain. DOLORES (Device Optimized for the LOw RESolution) was used, which is a focal reducer instrument of the TNG. The CCD used has a pixel size of 13.5 μm and the instrument has a field of view of 8.6' x 8.6'. The LR-B grism device and 1.5" slit were selected for observations, providing spectra with a resolution of about R = 500 for the 0.30-0.84 μm range. The slit was oriented along the parallactic angle, and the tracking followed the asteroid orbital motion, extracted from the corresponding ephemeris. Asteroid ephemerides were taken from the Minor Planet Center and objects were identified at the predicted position with the predicted proper motion (differential rates) at the time of observations. Three acquisitions offsetting the object 10" along the slit direction were obtained and subsequently averaged. The offsets

allowed measurement of the underlying sky flat, which was subtracted in the reduction process. **Table 1** lists each asteroid, date observed, apparent visual magnitude (m_v), exposure time, airmass, and solar analog used for data reduction (later discussed in Section 3.1). These observations taken on the TNG will now be referred to as Data Set 1.

Table 1: List of B-type asteroids observed from February 6, 2012 to February 8, 2012 on the Telescopio Nazionale Galileo (TNG) (Data Set 1).

Asteroid	Date Observed	m_v	Exposure Time (s)	Airmass	Solar Analog*
(45) Eugenia	7-Feb-2012	12.4	300	1.21	1,2
(47) Aglaja	6-Feb-2012	12.4	600	1.37	1,2
(62) Erato	6-Feb-2012	14.3	600	1.24	1,2
(88) Thisbe	6-Feb-2012	12.6	300	1.18	1,2
(213) Lilaea	7-Feb-2012	14.5	400	1.07	1,2
(225) Henrietta	6-Feb-2012	14.4	600	1.36	1,2
(229) Adelinda	6-Feb-2012	15.4	600	1.17	1,2
(268) Adorea	7-Feb-2012	11.9	300	1.33	1,2
(314) Rosalia	7-Feb-2012	15.6	800	1.45	1,2
(379) Huenna	7-Feb-2012	14.6	600	1.26	1,2
(419) Aurelia	7-Feb-2012	12.9	300	1.17	1,2
(426) Hippo	6-Feb-2012	14.1	600	1.12	1,2
(461) Saskia	7-Feb-2012	15.7	600	1.25	1,2
(468) Lina	6-Feb-2012	16.2	600	1.03	1,2
(555) Norma	6-Feb-2012	16.1	600	1.40	1,2
(747) Winchester	7-Feb-2012	13.6	600	1.07	1,2
(757) Portlandia	8-Feb-2012	14.9	400	1.12	1
(936) Kunigunde	7-Feb-2012	16.3	600	1.04	1,2
(954) Li	7-Feb-2012	14.7	600	1.15	1,2

Note: Solar analogs used include (1) Hyades 64, (2) Landolt 102-1081

2.1 Additional Observations

Additional observations, listed below in **Table 2**, were provided by Javier Licandro for a more complete survey of B-type asteroids, which will from now on be referred to as Data Set 2. Select spectra were published in Licandro et al. (2011) and the remaining spectra are unpublished. These supplementary observations were obtained with the 4.2-m William Herschel Telescope (WHT) and the 2.5-m Isaac Newton Telescope (INT), which are also located in La Palma, Spain.

Spectra of asteroids (62) Erato, (379) Huenna, and (383) Janina – all members of the Themis asteroid family – were obtained by Licandro et al. (2011) on April 1, 2006 with the WHT. The ISIS spectrograph was used with a 5" slit that was oriented in the parallactic angle. Spectra in the red and blue arms were obtained simultaneously using the R300B and R158R gratings, respectively. The rest of the objects, which are also members of the Themis family, were observed on three separate nights in 2007 with the IDS spectrograph at the INT, using a 5" slit and the R150V grism. The observational procedure followed to obtain these extra spectra is the same as that described for Data Set 1(Section 2).

Table 2: List of additional observations using the William Herschel Telescope (WHT) and the Isaac Newton Telescope (INT) in La Palma, Spain (Data Set 2).

Asteroid	Date Observed	Telescope Used	Solar Analog*
(62) Erato	1-Apr-2006	WHT	3,4
(316) Goberta	3-May-2007	INT	2,3
(379) Huenna	1-Apr-2006	WHT	3,4
(383) Janina	1-Apr-2006	WHT	3,4
(461) Saskia	24-Apr-2007	INT	3
(621) Werdandi	3-May-2007	INT	2,3
(936) Kunigunde	24-Apr-2007	INT	3
(1623) Vivian	3-May-2007	INT	2,3
(1687) Glarona	3-May-2007	INT	2,3
(2489) Suvorov	24-Apr-2007	INT	3
(2524) Budovicium	24-Apr-2007	INT	3
(6301) 1989 BR1	3-May-2007	INT	2,3

* ***Note:*** Solar analogs used include (2) Landolt 102-1081, (3) Landolt 107-684, and (4) BS 4486.

It is interesting to note that asteroids (62) Erato, (379) Huenna, (461) Saskia, and (936) Kunigunde overlap between Data Sets 1 and 2. Therefore, additional observations from Data Set 2 provide a clearer picture of these asteroids in a similar wavelength range but on different telescopes with different viewing conditions.

3 Data Reduction

Data reduction of Data Set 1 was executed using the Image Reduction and Analysis

Facility (IRAF) by first applying standard bias and flat-field corrections to the images. One-dimensional spectra were then extracted, and wavelength calibration was performed using the observed standard arc lamps to convert pixel number to wavelength. Arc lamp emission lines were identified using a comparison spectrum of known lines, and a best fit of wavelength as a function of pixel was calculated. The unique dispersion solution for each night was then applied to the asteroid and solar analog spectra, outputting spectra of intensity versus wavelength. Lastly, multiple frames were combined using average values to produce one spectrum of each object.

3.1 Solar Analog Analysis

Each asteroid spectrum was divided by corresponding solar analog spectra to remove the incident spectrum of the Sun and leave behind only the intrinsic reflectance of the asteroid. The solar analogs observed on each night of new observations are listed below in Table 3. Whenever possible, solar analogs and asteroids were observed at the same airmass to minimize the effects of differential atmospheric refraction on the spectral slopes of the objects. The solar analogs from the Landolt catalog (Landolt, 1992) have been previously tested as good solar analogs and have been extensively used in observations to obtain both visible and near-infrared spectra of asteroids (Bus and Binzel, 2002). Hyades 64 (not included in the Landolt catalog) was studied in the near-UV by Hardorp (1978) and identified as a good solar analog in this wavelength region. Therefore, Hyades 64 was intentionally selected as a reference star to compare to the other Landolt stars in determining their accuracy as solar analogs.

Table 3: List of solar analogs used for new observations each night and their corresponding airmass. Hyades 64 was first analyzed by Hardorp (1976). All other solar analogs are from the Landolt catalog (Landolt, 1992).

	Solar Analog	Airmass
06-Feb-2012	Hyades 64	1.18
	Landolt 102-1081	1.25
	Landolt 107-684	1.33
	Landolt 98-978	1.14
07-Feb-2012	Hyades 64	1.21
	Landolt 102-1081	1.18
	Landolt 107-684	1.29
	Landolt 98-978	1.15

08-Feb-2012	Hyades 64	1.09
	Landolt 98-978	1.16

As noted in **Table 1** (Section 2), only Hyades 64 and Landolt 102-1081 were used for solar analog division for the three nights of our new observations. The two remaining solar analogs were rejected for the reasons listed below:

1. First, after taking all asteroids and dividing them by each solar analog (normalizing spectra to unity at 5500 Å), features were still present in specific solar line regions. These regions include the solar G iron line at 4308 Å, and the solar H and K calcium lines at 3968 and 3934 Å respectively.

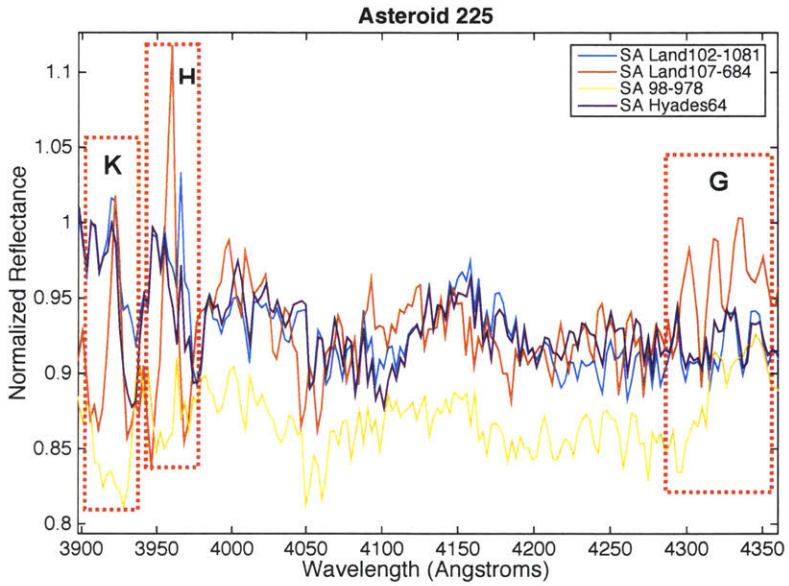

Fig. 1: An example of Asteroid 225 divided by each observed solar analog. The region around the solar G iron line at 4308 Å and the regions around the solar H and K calcium lines at 3968 and 3934 Å are highlighted in the red dashed boxes. If the solar analogs truly behaved like the sun, no features or peaks would be present in those regions. However, peaks are visible for SA (Solar Analog) Landolt 107-684 (red) and Landolt 98-978 (yellow). The same behavior can be seen in all asteroids.

If the observed solar analogs behave like the Sun, these features should disappear from the asteroid spectra after division. However, peaks are still present in these

regions for solar analog (SA) Landolt 107-684 and Landolt 98-978, shown in red and yellow respectively in **Fig. 1**.

2. The second reason for only using Hyades 64 and Landolt 102-1081 is that the other two solar analogs introduced significant changes in spectral slopes. True solar analogs should not contribute to changes in spectral slope, and these changes should instead come directly from the asteroid itself. However, after dividing every asteroid by each solar analog, significant variations in slope were observed for Landolt 107-684 and 98-978, as seen below in **Fig. 2**. This is especially visible in the 6000-8000 Å range, where Landolt 107-684 (red) introduces a downward slope and Landolt 98-978 (yellow) introduces an upward slope.

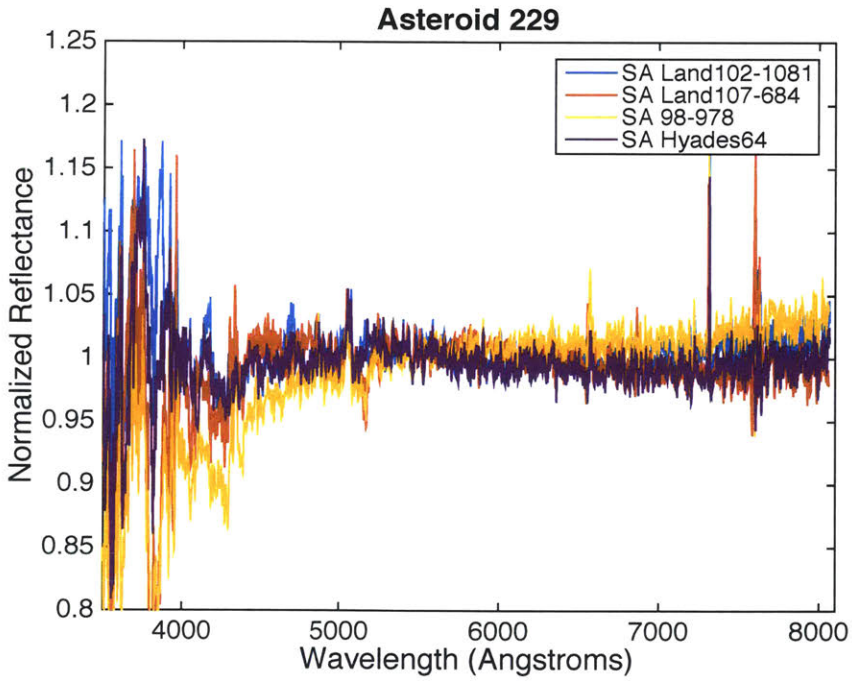

Fig. 2: An example of Asteroid 229 divided by each observed solar analog from 3500-8000 Å. Solar analogs Landolt 107-684 (red) and 98-978 (yellow) introduce significant spectral slope changes, deviating from mean spectra. This deviation can be seen more clearly from the 6000-8000 Å range, where Landolt 107-684 introduces a downward slope and Landolt 98-978 introduces an upward slope.

One may be tempted to attribute these variations in spectral slope to the differences in airmass between the asteroids and the solar analogs. However, we see the same solar analog behavior for all the asteroids and on both nights.

3. To further illustrate changes in spectral slope due to solar analogs, dispersions in spectral slope were lastly calculated for each star. Dispersions in slope show the percent difference from a value of 1 per 1000 Å. Theoretically, if each solar analog is divided by each other, the resulting spectra should be a horizontal line at a constant value of 1 since solar analogs ideally should be identical to each other and to the sun. A more realistic assumption that not all solar analogs are identical allows for an acceptable dispersion of less than 1% per 1000 Å (Lazzaro et al., 2004). Dispersions for each solar analog compared to Hyades 64 (used as a reference) are illustrated below in **Fig. 3**, where linear fits for each spectrum (green) and the expected horizontal line at a value of 1 (dashed black) are displayed. We have computed the dispersions in the two regions of interests, i.e., 3800-5500 Å and 5500-8000Å. The obtained values are shown in Table 3.

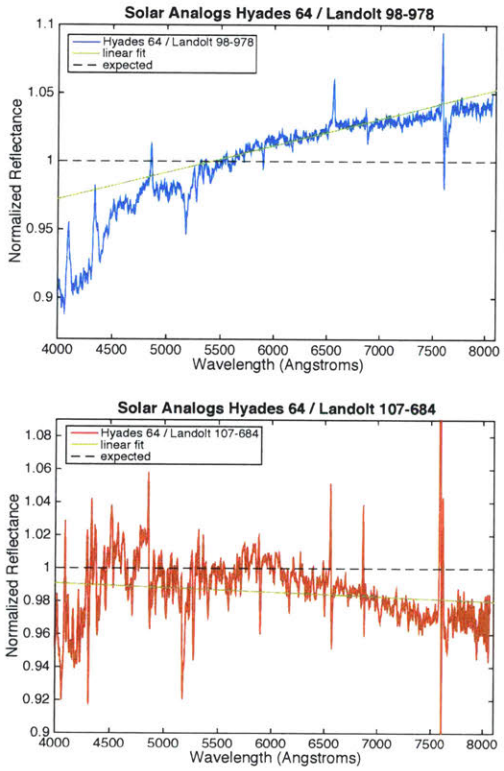

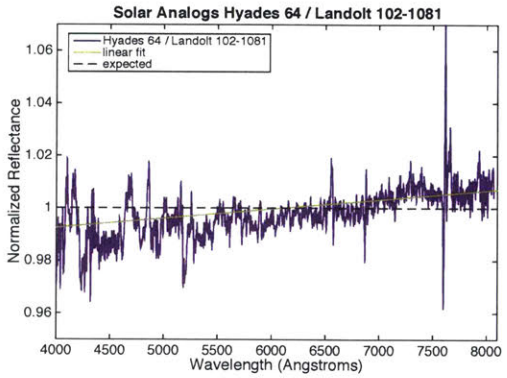

Fig. 3: Solar analog Hyades 64 divided by remaining solar analogs (taken as mean spectra from 06 Feb. and 07 Feb. 2012). Since solar analogs should be identical, it is expected that the resulting spectra will be a flat line at a value of 1 (dashed black). However, linear fits (green) reveal dispersions away from the value of 1 for each solar analog.

Table 3: The mean percent dispersion per 1000 Å for Hyades 64 divided by each solar analog. Values were calculated by taking the mean spectra from 2 nights (06 Feb. and 07 Feb. 2012). Percent dispersion per 1000 A represents the deviation from a value of 1 at intervals of 1000 Å from 3800-8000 Å.

Hyades 64 / Solar Analog	Mean % Dispersion per 1000 Å (3800-5500 Å)	Mean % Dispersion per 1000 Å (5500-8000 Å)	Mean slope (%/1000 Å) (3800-8000Å)
Landolt 98-978	9.14%	1.52%	4.29
Landolt 102-1081	2.00%	0.40%	0.08
Landolt 107-684	7.15%	1.33%	0.39

By looking at **Fig. 3** and **Table 3**, it is clear that Landolt 102-1081 is the most acceptable solar analog with a mean percent dispersion per 1000 Å of less than 1% for the entire wavelength range (3000-8000 Å) and slightly above 1% for the near-UV region. Landolt 107-684 behaves well above 5500 Å, with a dispersion of 1.3%/1000 Å, but presents serious problems in the near-UV region. Landolt 98-978 is evidently the worst solar analog of the sample with a significantly higher mean percent dispersion for boththe near-UV region and the entire wavelength range.

It is possible that the large slope differences between the standard solar analog Hyades 64 and the other solar analogs, especially Landolt 98-978, was due to atmospheric extinction. When objects are observed at different airmasses (denoted in **Table 3**), different atmospheric effects can scatter light and alter observations. An atmospheric extinction curve (King, 1985) for the El Roque de Los Muchachos Observatory, where the TNG is located, was applied to solar analog observations for the 3 nights of Data Set 1. However, as seen in **Fig. 4**, significant changes were not found in the spectral slopes of solar analogs after applying atmospheric extinction corrections. Therefore, the spectral slope dispersions illustrated in **Fig. 3** and **Table 3** were due to the solar analogs rather than observational effects.

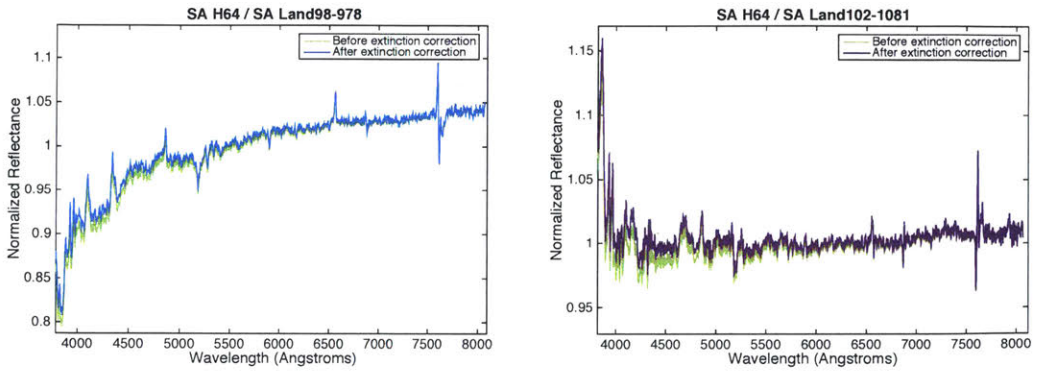

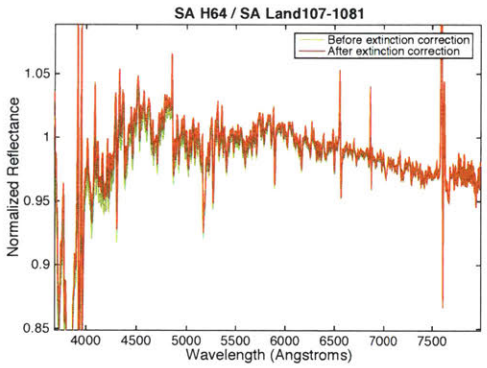

Fig. 4: Solar analog Hyades 64 divided by remaining solar analogs before and after atmospheric extinction corrections. Solar analog spectral slopes did not change significantly after applying extinction corrections.

After observing the behavior of the four solar analogs in solar G, H, and K regions, inspecting the introduction of spectral slope changes and analyzing percent dispersions, it was concluded that Landolt 107-684 and Landolt 98-978 should not be used to obtain the final reflectance spectra of the asteroids observed at the TNG. Instead, Hyades 64 and Landolt 102-1081 were combined and used as solar analogs for the nights of February 6 and 7. On February 8, only Hyades 64 was used.

It is important to remark here that these solar analogs should not be used to obtain reflectance spectra in the near-UV region. Past studies indicate that Hyades 64, Landolt 102-1081, and Landolt 107-684 are appropriate and widely used solar analogs for spectral analysis in the visible and near-infrared. Barry (1978) and Barry and Cromwell (1976) found that the metallicities of the Hyades group of stars match identically with metallicities of the sun. Furthermore, Hardorp (1978) confirmed that Hyades 64 is a solar spectral analog in the near-UV and can therefore be used for the purposes of this study. Landolt 102-1081 was also used as a spectral solar analog for TNG observations conducted by Pinilla-Alonso et al. (2013), de León et al. (2012, 2010), Campins et al. (2007), Duffard et al. (2006), and Fornasier et al. (2004). In addition, Landolt 107-684 was used as a solar analog by Licandro et al. in 2011.

To complete the reduction process, Hyades 64 and Landolt 102-1081 were combined using average values. Each asteroid was then divided by the combined solar analog spectrum to yield final reflectance spectra. Reflectances were lastly normalized to unity at 5500 Å by convention. In the case of Data Set 2, observations were carried out using the WHT and published by Licandro et al. (2011) used Landolt 107-684 and BS4464 as solar

analogs (see Table 2). Unfortunately, we do not have access to the spectra of the stars to perform a similar analysis to that of our observations. However, for Data Set 2, only one solar analog was used in two of the nights, and two solar analogs (Landolt 102-1081 and Landolt 107-684) were used for the third night. In this last case, the dispersion introduced by the use of Landolt 107-684 with respect to Landolt 102-1081 is 11%/1000 Å for the 3800-5500 Å range and 0.98%/1000Å for the 5500-8000 Å range. Again, it is clear that the SA 107-684 should not be used if one is interested in the reflectance spectra of asteroids in the near-UV wavelength range.

4 Results

4.1 Reflectance Spectra

The resulting spectra of each asteroid are shown below as black lines in **Fig. 5**. Colored spectra represent observations from past studies, including the Small Main-Belt Asteroid Spectroscopic Survey (SMASS, Bus and Binzel, 2002), Eight Color Asteroid Survey (ECAS, Zellner et al., 2009), Sawyer Asteroid Spectra (Sawyer, 1998), and Small Solar System Objects Spectroscopic Survey (S3OS2, Lazzaro et al., 2006).

The observed spectra match past data relatively well with the exception of Asteroid (314) Rosalia. This object has a low signal-to-noise ratio (SNR) of 21.68 and is very noisy. It is also important to note that three frames of 800 seconds were taken of Asteroid (314) Rosalia, and the seeing continued to worsen throughout this time. Therefore, this asteroid was rejected from the sample, leaving a total of 18 asteroids for spectral slope analysis.

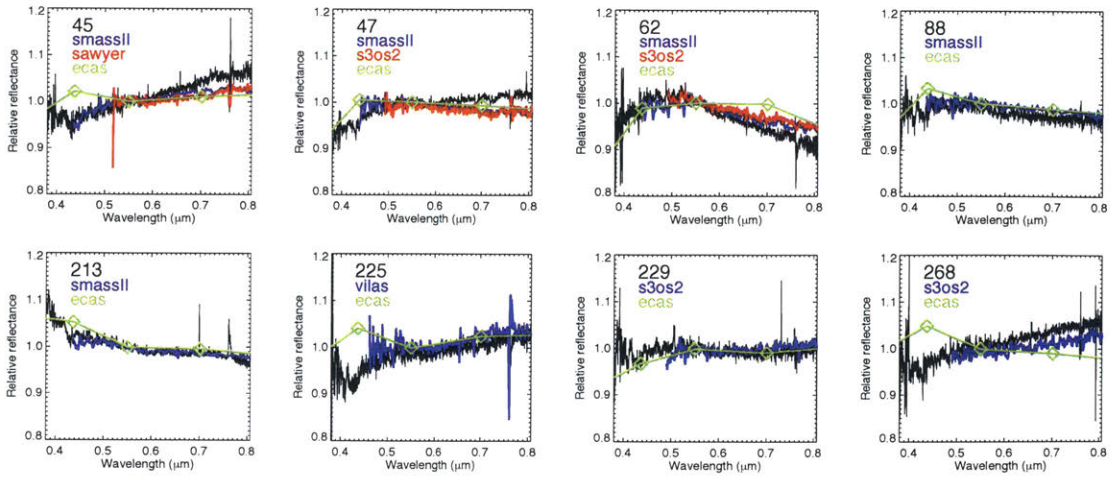

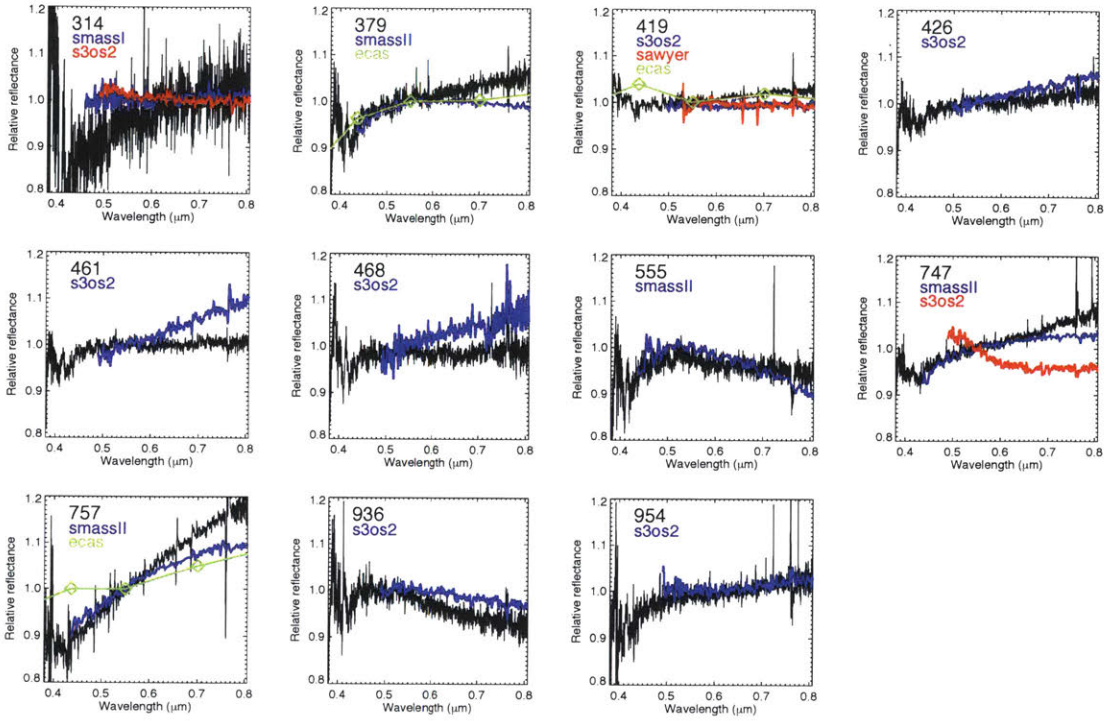

Fig. 5: Reflectance spectra of all asteroids from observations using the Telescopio Nazionale Galileo (TNG) on February 6-8, 2012 (Data Set 1) (black). Spectra from previous studies are overlaid in colors including the Small Main-Belt Asteroid Spectroscopic Survey (SMASS, Bus and Binzel, 2002), Eight Color Asteroid Survey (ECAS, Zellner et al., 2009), Sawyer Asteroid Spectra (Sawyer, 1998), and Small Solar System Objects Spectroscopic Survey (S3OS2, Lazzaro et al., 2006).

A similar plot of the additional observations is shown below in **Fig. 6**. The same legend is used as before, where colored spectra represent observations from past studies, including the Small Main-Belt Asteroid Spectroscopic Survey (SMASS, Bus and Binzel, 2002), Eight Color Asteroid Survey (ECAS, Zellner et al., 2009), Sawyer Asteroid Spectra (Sawyer, 1998), and Small Solar System Objects Spectroscopic Survey (S3OS2, Lazzaro et al., 2006). No past observations were found for asteroids (1623) Vivian, (1687) Glarona, and (6301) 1989 BR1.

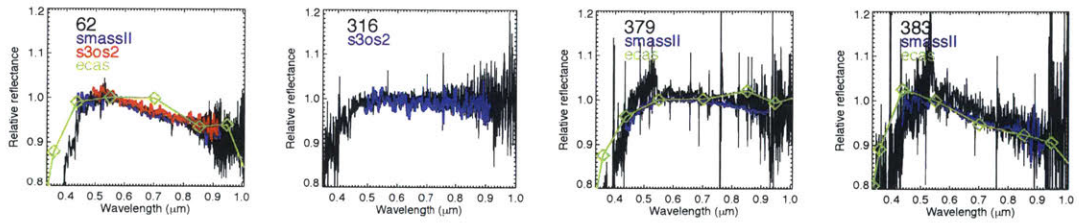

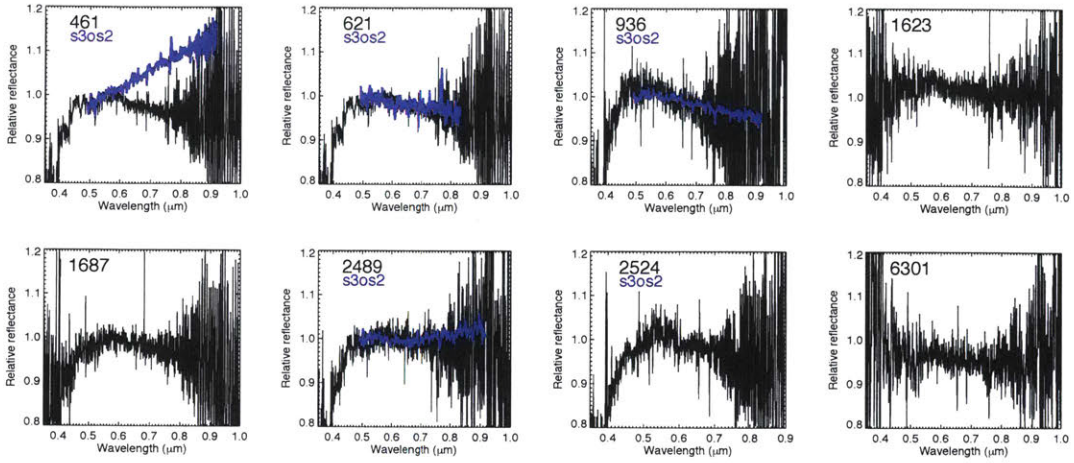

Fig. 6: Reflectance spectra of additional observations using the William Herschel Telescope (WHT) and Isaac Newton Telescope (INT) (Data Set 2) (black). Spectra from previous studies are overlaid in colors including the Small Main-Belt Asteroid Spectroscopic Survey (SMASS, Bus and Binzel, 2002), Eight Color Asteroid Survey (ECAS, Zellner et al., 2009), Sawyer Asteroid Spectra (Sawyer, 1998), and Small Solar System Objects Spectroscopic Survey (S3OS2, Lazzaro et al., 2006).

4.2. Common Objects Between Data Sets

In **Fig. 7** below, the asteroids that are included in both Data Sets 1 and 2 are overlaid to better compare their spectra. TNG observations are shown in blue and additional observations are shown in red and yellow. Asteroids (62) and (379) (in red) are distinguished from asteroids (461) and (936) (in yellow) due to the fact that different solar analogs were used to reduce their spectra. In the TNG observations, Hyades 64 and Landolt 102-1081 were used for reduction, whereas in the additional observations on the WHT used both Landolt 107-684 and BS 4486 as solar analogs. Thus systematic effects can be present when we compare reflectance spectra from the two observations; however, it is useful to visualize their differences. For asteroids (461) and (936) (shown in yellow), this inaccuracy is not the case. The data taken with the INT used Landolt 107-684. Therefore, we show in Fig. 7 the resulting spectra for the same asteroids observed at the TNG using the same solar analog, only for comparison purposes. The similarity in the case of asteroid (461) is remarkable. These examples illustrate how important is the correct selection of the solar analogs, and how differences in the reduction process or even in the observation site can affect the slope of the reflectance spectra of the

asteroids. This can also be seen in Figs. 5 and 6 where previously published spectra are overlaid and differences are significant in some of the cases.

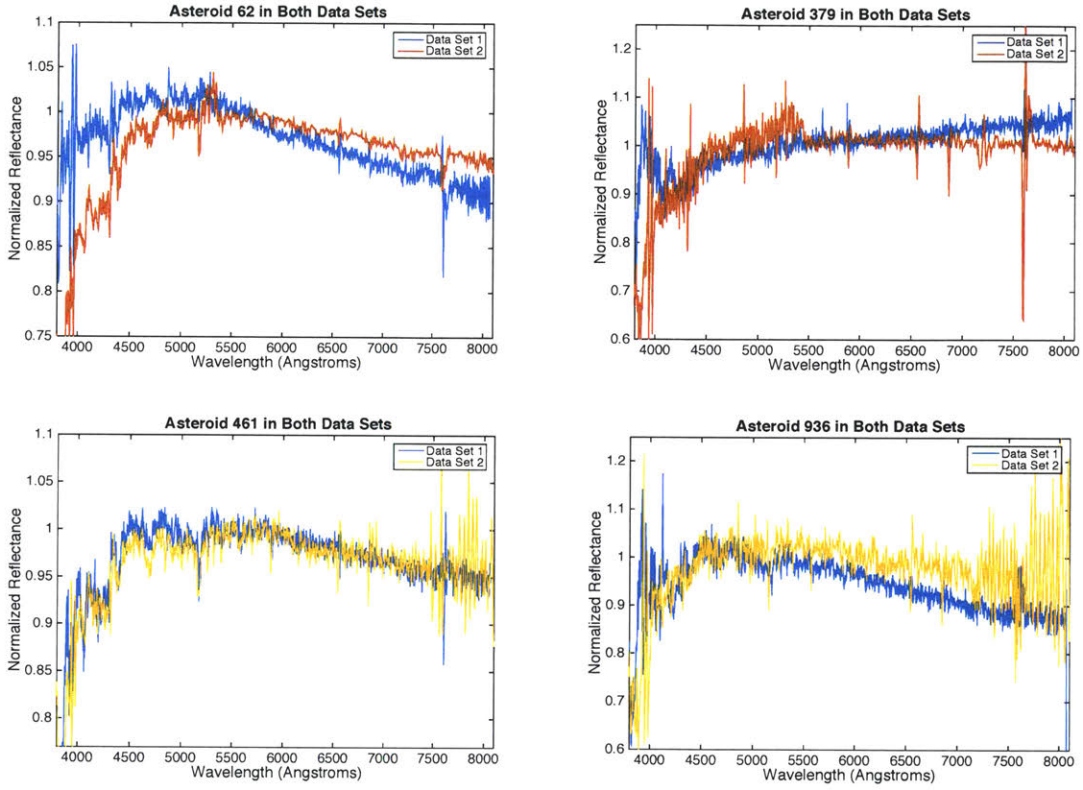

Fig. 7: Reflectance spectra of the asteroids that appear in both data sets. The additional observations (Data Set 2) of asteroids (62) and (379) (in red) used both Landolt 107-684 and BS 4486 for reduction, while our data with the TNG used Hyades 64 and Landolt 102-1081. Therefore, systematic effects based on the use of different solar analogs can affect the comparison of the spectra plotted in red and blue. Additional observations of asteroids (461) and (936) in Data Set 2 were reduced only using Landolt 107-684. In this case, and only for the comparison in this section, we used Landolt 107-684 to obtain the spectra of asteroids (461) and (936).

4.3 Spectral Slope Calculations

The resulting spectra shown in **Figs. 5** and **6** exhibit a drop-off in reflectance shortwards of 5500 Å, attributed to the presence of an absorption band in the ultraviolet wavelength region. Therefore, the spectral analysis in this work was split into two regions: 1) 3800-5500 Å and 2) 5500-8000 Å.

Slopes of the reflectance spectra of all asteroids were calculated for the two regions mentioned. The procedure involved fixing a point at unity at 5500 Å (since all spectra were normalized to this value at 5500 Å) and picking 5 points around the low bound of

3800 Å and the high bound of 8000 Å. The points around 3800 Å were connected to the fixed point at 5500 Å using straight lines, and similarly for the points around 8000 Å. Slopes were then calculated for each line, and an average slope for each region was calculated. This procedure was then repeated for each asteroid in the sample. The calculated slopes are presented below in **Table 4**, grouped by data sets.

Table 4: Slopes (in %/1000Å) of reflectance spectra from each asteroid for the two regions of interest: 1) 3800-5500 Å and 2) 5500-8000 Å. Errors were calculated as standard deviations. Data are grouped by observations with new observations with the TNG listed first (Data Set 1) and additional observations with the WHT and INT second (Data Set 2).

Data Set 1 (TNG)

Asteroid	Slope 1 (3800-5500 Å)	Error	Slope 2 (5500-8000 Å)	Error
(45) Eugenia	2.276	1.744	2.568	0.244
(47) Aglaja	5.120	0.970	0.656	0.067
(62) Erato	5.818	2.137	-3.455	0.619
(88) Thisbe	2.945	0.747	-1.459	0.359
(213) Lilaea	-4.736	0.753	-1.425	0.185
(225) Henrietta	7.093	1.816	1.192	0.379
(229) Adelinda	1.240	1.463	-0.603	0.466
(268) Adorea	4.824	0.968	2.384	0.350
(379) Huenna	7.943	2.369	2.578	0.159
(419) Aurelia	-0.424	0.412	1.024	0.213
(426) Hippo	3.640	0.292	0.727	0.590
(461) Saskia	7.198	1.838	0.504	0.286
(468) Lina	2.592	1.423	-0.741	0.720
(555) Norma	11.125	4.446	-2.277	1.049
(747) Winchester	14.565	0.794	3.091	0.468
(757) Portlandia	14.565	2.556	7.537	0.569
(936) Kunigunde	5.260	3.654	-2.435	1.354
(954) Li	7.591	1.589	1.160	0.791

Data Set 2 (WHT, INT)

Asteroid	Slope 1 (3800-5500 Å)	Error	Slope 2 (5500-8000 Å)	Error
(62) Erato	15.652	0.868	-2.066	0.226
(316) Goberta	6.891	2.665	0.104	0.415
(379) Huenna	16.056	0.930	-0.061	0.644

(383) Janina	12.186	7.336	-2.032	1.555
(461) Saskia	10.436	0.930	-2.394	0.644
(621) Werdandi	0.012	2.224	0.856	1.129
(936) Kunigunde	17.156	4.416	-2.394	7.385
(1623) Vivian	4.752	3.325	-1.021	2.106
(1687) Glarona	9.963	4.750	-1.532	1.721
(2489) Suvorov	14.554	1.807	-2.533	2.158
(2523) Budovicium	16.326	5.184	-4.663	1.844
(6301) 1989 BR1	2.343	7.838	-3.559	1.622

5 Discussion

5.1 Spectral Taxonomies

We have presented our resulting spectra in **Figs. 5** and **6**. According to Bus and Binzel (2002a,b), B-type asteroids present "linear, featureless spectra over the interval from 0.44 to 0.92 μm, with negative (blue) to flat slopes." However, not all the spectra presented in **Figs. 5** and **6** fit into this definition. To determine which asteroids fit, selection criteria were used to determine if spectra from new observations followed Bus and Binzel taxonomy. The selection criteria are consistent with that used by de León et al. (2012): asteroids with published visible spectra designated as F- or B-type, including ambiguous designations, according to the most commonly used taxonomies (Tholen, 1984; Bus and Binzel, 2002a,b). F-types, which also fall into the wider group of carbonaceous asteroids, are mainly differentiated from B-types by the fact that their spectra show a much weaker drop-off in the ultraviolet. Furthermore, B-types show a moderately higher average albedo than F-types. It is important to note that the above criteria were not used to select the additional asteroids in Data Set 2 designated in **Table 2** (Section 2.1). These objects were instead chosen for being members of the Themis collisional family, as mentioned previously.

Columns 2 and 3 of **Table 5** show Tholen's (1984) and Bus and Binzel's (2002a,b) taxonomic classifications of our set of asteroids from previous observations. The last column represents taxonomic classifications generated using the M4AST online classification tool (Popescu et al., 2012) by inputting our observed spectra. This simple tool works by first uploading an asteroid reflectance spectrum. The tool then fits a curve to the spectrum and compares it to the taxonomic classes defined by Bus and Binzel

(2002a,b) at corresponding wavelengths using a χ^2 procedure. The 5 best results of taxonomic classifications are lastly output in order of increasing standard deviation. The same tool was used to classify Data Set 2.

Table 5: Previous taxonomic classifications using Tholen (1984) and Bus and Binzel (2002a,b) of all asteroids in this study, grouped by observations. The last column represents taxonomic classifications generated using the M4AST online classification tool by inputting our spectra.

	Taxonomy		
Asteroid	**Tholen**	**Bus**	**M4AST**
Data Set 1 (TNG):			
(45) Eugenia	FC	C	X
(47) Aglaja	C	B	C
(62) Erato	BU	Ch	B
(88) Thisbe	CF	B	B
(213) Lilaea	F	B	B
(225) Henrietta		B	C
(229) Adelinda	BCU	Cb	C/B*
(268) Adorea	FC	X	C/X*
(379) Huenna	B	C	C/X*
(419) Aurelia	F	Cb	Cb
(426) Hippo	F	X	C
(461) Saskia	FCX	X	C
(468) Lina	CPF	Xk	C
(555) Norma		B	B
(747) Winchester	PC	C	X
(757) Portlandia	XF	Xk	T
(936) Kunigunde	B	B	B
(954) Li	FCX	Cb	C
Data Set 2 (WHT, INT):			
(62) Erato	BU	Ch	B
(316) Goberta	C	C	B
(379) Huenna	B	C	B
(383) Janina	B	B	B
(461) Saskia	FCX	X	B
(621) Werdandi	B	B	B
(936) Kunigunde	B	B	B
(1623) Vivian		B	B
(1687) Glarona		B	B
(2489) Suvorov		X	B

(2523) Budovicium	B	B	B
(6301) 1989 BR1		B	B

**Note:* The two different taxonomic classifications produce the same χ^2 value, so both are considered.

A variety of asteroids can be seen in the table above, indicating that not all asteroids in this study correspond with Bus and Binzel's earlier description of B-types. However, it is important to note that differences in taxonomies between the Tholen, Bus, and M4AST data sets are not significant. Although letters may differ, the characteristics of these asteroids are still similar. For example, two spectra can be nearly identical, but due to the fact that formal classification uses a simple system of cutoffs to differentiate spectra, any minute variations in the two spectra can lead to different final taxonomies.

For consistency, we only consider those asteroids classified as B-types using the M4AST tool for analysis. A final list of the 14 B-type asteroids used for further analysis is included in **Table 6** below. More specifically, asteroids (379) Huenna and (461) Saskia were not included in this final list since their spectra in Data Set 1 were not classified as B-types using the M4AST tool. The reflectance spectra of these selected B-types are additionally presented in **Figs. 8** and **9** below.

Table 6: Final list of 14 asteroids used for analysis. For consistency, only asteroids that were classified as B-type through the M4AST tool were selected.

	Taxonomy		
Asteroid	**Tholen**	**Bus**	**M4AST**
Data Set 1 (TNG):			
(62) Erato	BU	Ch	B
(88) Thisbe	CF	B	B
(213) Lilaea	F	B	B
(229) Adelinda	BCU	Cb	B
(555) Norma		B	B
(936) Kunigunde	B	B	B
Data Set 2 (WHT, INT):			
(62) Erato	BU	Ch	B
(316) Goberta	C	C	B
(383) Janina	B	B	B
(936) Kunigunde	B	B	B

(621) Werdandi	B	B	B
(1623) Vivian		B	B
(1687) Glarona		B	B
(2489) Suvorov		X	B
(2523) Budovicium	B	B	B
(6301) 1989 BR1		B	B

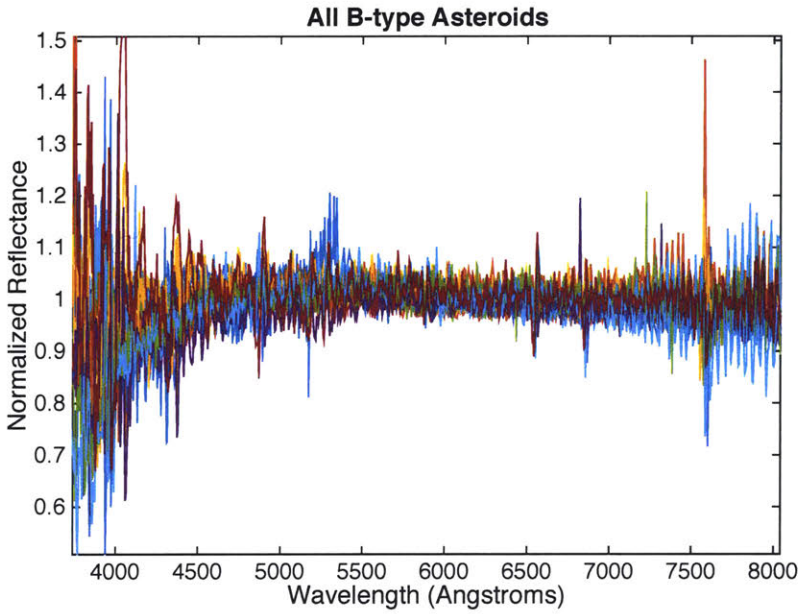

Fig. 8: Reflectance spectra of the 14 asteroids classified as B-types using the M4AST tool.

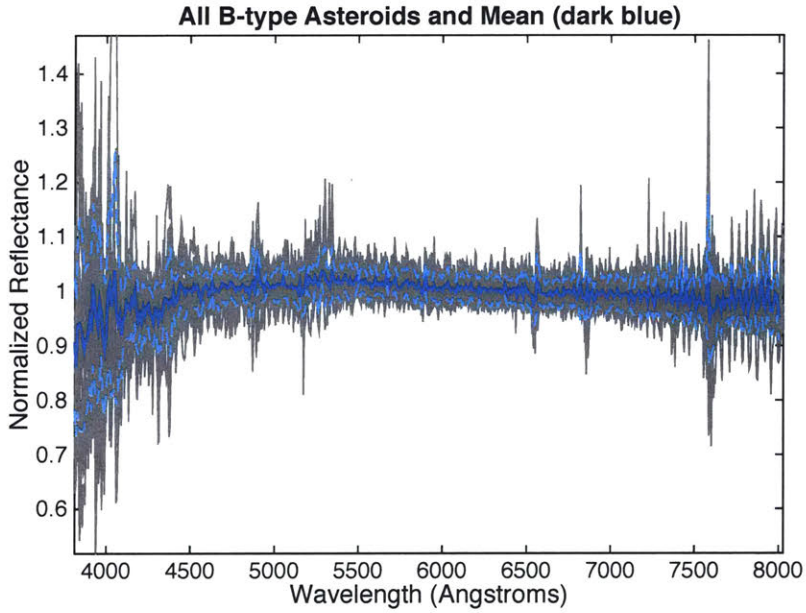

Fig. 9: Same reflectance spectra of the 14 B-type asteroids (grey) overplotted by the mean

spectrum (dark blue) and ±1 σ of the mean (light blue).

5.2 Spectral Slope Variations

Through visual inspection of **Figs. 8** and **9**, it is evident that a variation in spectral slope exists between the 14 B-type asteroids in this data set. To quantify this variation, spectral slopes calculated in the previous section are presented below in **Table 7**.

Table 7: An updated list of asteroids from **Table 5** classified as B-types using the M4AST online tool and their spectral slopes in two wavelength regions. The slopes are in units of %/1000 Å.

Data Set 1 (TNG)

Asteroid	Slope 1 (3800-5500 Å)	Error	Slope 2 (5500-8000 Å)	Error
(62) Erato	5.818	2.137	-3.455	0.619
(88) Thisbe	2.945	0.747	-1.459	0.359
(213) Lilaea	-4.736	0.753	-1.425	0.185
(229) Adelinda	1.240	1.463	-0.603	1.007
(555) Norma	11.125	4.446	-2.277	1.049
(936) Kunigunde	5.26	3.654	-2.435	1.354

Data Set 2 (WHT, INT)

Asteroid	Slope 1 (3800-5500 Å)	Error	Slope 2 (5500-8000 Å)	Error
(316) Goberta	6.891	2.665	0.104	0.415
(383) Janina	12.186	7.336	-2.032	1.555
(621) Werdandi	0.012	2.224	0.856	1.129
(1623) Vivian	4.752	3.325	-1.021	2.106
(1687) Glarona	9.963	4.75	-1.532	1.721
(2489) Suvorov	14.554	1.807	-2.533	2.158
(2523) Budovicium	16.326	5.184	-4.663	1.844
(6301) 1989 BR1	2.343	7.838	-3.559	1.622

Spectral slopes from **Table 7** were further analyzed by computing the variations in slopes within each wavelength region (3800-5500 Å and 5500-8000 Å). As seen below in **Table 8**, the minimum and maximum slope values of those listed in **Table 7** were identified for each region.

Table 8: The minimum and maximum slopes of the 14 B-type asteroids used for this study in each of the wavelength regions. All B-types were included to calculate variations in the top half of the table. The bottom half calculates variations excluding asteroids that used only Landolt 107-684 as a solar analog for reduction, which are (383) Janina, (2489) Suvorov, and (2524) Budovicium.

All B-type asteroids		
	Slope 1 (3800-5500 Å)	**Slope 2 (5500-8000 Å)**
Maximum	16.326	0.856
Minimum	-4.736	-4.663
Variation	21.06%	5.52%

Excluding asteroids obtained using only Landolt 107-684		
	Slope 1 (3800-5500 Å)	**Slope 2 (5500-8000 Å)**
Maximum	11.125	0.856
Minimum	-4.736	-3.559
Variation	15.86%	4.42%

The variation in spectral slope seen in the two regions of interest is significantly larger than the variations introduced by the solar analogs (**Table 3**, Section 3.1). For Data Set 1, solar analogs Landolt 102-1081 and Hyades 64 were used for spectral reduction. This combination of solar analogs introduces a change in spectral slope of 2%/1000Å in the near-UV. Even in the worst case, where only Landolt 107-684 would have been used to obtain the reflectance spectra of the asteroids, the variation introduced by this solar analog would have been 7%/1000 Å. The slope variation shown by the asteroids in that region almost triples this value (21%/1000Å).

In the case of the objects in Data Set 2 that used BS 4486 as the solar analog, we cannot compute the change introduced by this star since we lack access to its spectra. For the remaining objects in Data Set 2, though, the variation in spectral slope is about 16%/1000 Å in the 3800-5500 Å range, as noted in **Table 8**.

In Section 3.1, it was noted that Landolt 98-978 was not used as a solar analog for possessing features in solar regions and introducing significant variations in spectral slope. Based on these criteria, Hyades 64 and Landolt 102-1081 proved to be the "best solar analogs" in this sample and were used for reduction of Data Set 1. Although it was not the "worst" solar analog of the four, Landolt 107-684 was not used for data reduction. However, the additional observations included in Data Set 2 consistently used Landolt 107-684 as a solar analog, so it is interesting to focus on the behavior of this star..

Looking at the spectral slope values in the 3800-5500 Å region of **Table 7**, it is interesting that the largest values (> 12%/1000Å) are produced by spectra that used Landolt 107-684 for reduction, namely (383) Janina, (2489) Suvorov, and (2524) Budovicium. The spectra of these three asteroids in **Fig. 6** exhibit an anomalously sharp drop-off in reflectance below 5500 Å. This behavior could be traced to the use of Landolt 107-684 as a solar analog. If these three asteroids are not included, as calculated in **Table 8**, the variation in spectral slope for this wavelength region is smaller, but still significant.

Variations in spectral slope within these selected B-types are present, especially within the 3800-5500 Å near-ultraviolet region. These results support the work of de León et al. (2012), who found a continuous shape variation in spectral slope in the near-infrared region. This work also aligns with Alí-Lagoa's findings, which suggest that B-type asteroids have a similar behavior in the infrared region.

As discussed previously, variations have been very carefully controlled to minimize any contribution by solar analogs, since the dispersions of these solar analogs are significantly lower than spectral variations of the asteroids. Furthermore, variations are still present despite excluding spectra that used Landolt 107-684 as solar analog based on large spectral slope values. Additionally, slope variations do not appear to be attributable to observations taken at different airmasses, as discussed in Section 3.1.

If these variations are in fact real, what could they be revealing about the compositions or nature of these particular asteroid surfaces? As mentioned in the introduction, B-type asteroids have been linked to carbonaceous chondrites, mainly due to their similar spectra in the visible and near-infrared wavelength regions (Licandro et al., 2007; de León et al., 2012; Clark et al., 2010; Vilas and Gaffey, 1989; Vilas et al., 1994). In order to compare the spectral slope variations of the B-type asteroids analyzed in this work, we have computed the spectral slope in the 3800-5500 Å region for a sample of carbonaceous chondrites. The spectra of the meteorites were taken from the RELAB public database (Pieters and Hiroi 2004), and normalized to unity at 5500 Å for comparison purposes. The selected sample of carbonaceous chondrites contains all groups, spanning from the most aqueously altered and compositionally primitive CI/CM group to the dry, thermal metamorphism suffered by the CK chondrites. Interestingly, we found that the variation in spectral slope for the carbonaceous chondrites is about 15-25%/1000 Å, which is in good agreement with the slope variation observed for the B-types in the same wavelength region.

In general, CI/CM chondrites show the highest values of spectral slope in the 3800-5500 Å region. Meteorites analyzed include samples that have been heated to different degrees. It is interesting to note that, independently of the meteorite group, as temperature increases, the spectral slope decreases; this is a result of the decrease in depth of the UV absorption band. Negative spectral slopes are computed only for samples heated above 700°C. In the same way, increasing grain size produces a similar effect in the spectral slope, although the change in spectral slope is smaller than for the temperature case.

6 Conclusion

This study obtained new observations of 19 B-type asteroids using the Telescopio Nazionale Galileo (TNG) and included additional observations collected on the William Herschel Telescope (WHT) and Isaac Newton Telescope (INT), all at the El Roque de Los Muchachos Observatory. The use of appropriate solar analogs was integral to this study, and it was determined that Hyades 64 was the most suitable solar analog for spectral reduction, followed by Landolt 102-1081, Landolt 107-684 and Landolt 98-978.

Once spectra were reduced using the appropriate solar analogs, asteroids were classified using the M4AST online tool. Results showed that not all asteroids originally included in this study were true B-types. After excluding the non-B-type asteroids for analysis, spectral slopes and variations in spectral slopes were computed. It was found that variations in spectral slopes were present, and these variations could not be traced to the use of certain solar analogs or differences in airmass during observations. Furthermore, spectral slope variations of the B-type asteroids are in good agreement with spectral slope variations of carbonaceous chondrites, in particular in the near-UV region. Interestingly, spectral slopes vary from large values for the CI/CM chondrites, which show the highest degrees of aqueous alteration, to smaller values of the CV/CK chondrites, which present dry, thermal metamorphism. These results support the work of de León et al. (2012), who found a continuous shape variation in spectral slope in the near-infrared region and also Alí-Lagoa (2013), who found a similar variation in the infrared region.

7 References

Alí-Lagoa, V., de León, J., Licandro, J., Delbó, M., Campins, H., Pinilla-Alonso, N., Kelley, M.S. (2013). Physical properties of B-type asteroids from WISE data. *Astronomy & Astrophysics, 554,* A71.

Barry, D.C. (1978). Spectroscopic differences between solar-type cluster stars and the sun. *Astrophysical Journal, 219,* 942-946.

Barry, D.C., Cromwell, R.H., Schoolman, S.A. (1976). The Metallicity of the Sun Relative to Hyades and Coma Cluster Stars. *Bulletin of the American Astronomical Society, 8,* 524.

Bottke Jr., W.F., Cellino, A., Paolicchi, P., Binzel, R.P. (2003). An Overview of the Asteroids: The Asteroids III. *Perspective*, 3–15.

Bus, S. J., & Binzel, R. P. (2002a). Phase II of the Small Main-Belt Asteroid Spectroscopic Survey: The Observations. *Icarus, 158*, 106-145.

Bus, S. J., & Binzel, R. P. (2002b). Phase II of the Small Main-Belt Asteroid Spectroscopic Survey: A Feature-Based Taxonomy. *Icarus*, *158*, 146-177.

Campins, H., Licandro, J., Pinilla-Alonso, N., Ziffer, J., de León, J., Mothé-Diniz, T., Guerra, J.C. (2007) Nuclear Spectra of Comet 28P Neujmin 1. *The Astronomical Journal, 134,* 1626-1633.

Clark, B.E., Ziffer, J., Nesvorny, D., Campins, H., Rivkin, A., Hiroi, T., Barucci, M., Fulchignoni, M., Binzel, R.P., et al. (2010). Spectroscopy of B - type asteroids: Subgroups and meteorite analogs. *Journal of Geophysical Research*, *115,* E06005-6027.

de León, J., Pinilla-Alonso, N., Campins, H., Licandro, J., & Marzo, G. A. (2012) Near-infrared spectroscopic survey of B-type asteroids: Compositional analysis. *Icarus, 218,* 196-206.

de León, J., Licandro, J., Serra-Ricart, M., Pinilla-Alonso, N., Campins, H. (2010). Observations, compositional, and physical characterization of near-Earth and Mars-crosser asteroids from a spectroscopic survey. *Astronomy & Astrophysics, 517,* A23-A49.

Duffard, R., de león, J., Licandro, J., Lazzaro, D., Serra-Ricart, M. (2006). Basaltic asteroids in the Near-Earth Objects population: a mineralogical analysis. *Astronomy & Astrophysics, 456,* 775-781.

Fornasier, S., Dotto, E., Barucci, M.A., Barbieri, C. (2004). Water Ice on the Surface of the Large TNO 2004 DW. *Astronomy & Astrophysics, 422*, L43-L46.

Johnson, T.V., Fanale, F. (1973). Optical properties of carbonaceous chondrites and their relationship to asteroids. *J. Geophys. Res., 78*, 8507–8518.

King, D.L. (1985). Atmospheric Extinction at the Roque de los Muchachos Observatory, La Palma. *La Palma Technical Note, 31*.

Landolt, A.U. (1992). UBVRI photometric standard stars in the magnitude range 11.5 < V< 16.0 around the celestial equator. *Astronomical Journal, 104,* 340–491.

Lazzaro, D., Angeli, C.A., Carvano, J.M., Mothe-Diniz, T., Duffard, R., and Florczak, M. (2004). S3OS2: the visible spectroscopic survey of 820 asteroids. *Icarus*, *172,* 179.

Licandro, J., Campins, H., Tozzi, P., de León, J., Pinilla-Alonso, N., Boehnhardt, H., Hainaut, O.R. (2011). Testing the comet nature of main belt comets. The spectra of 133P/Elst-Pizarro and 176P/LINEAR. *Astronomy & Astrophysics, 532,* A65.

Licandro, J., Campins, H., Mothé-Diniz, T., Pinilla-Alonso, N., de León, J. (2007). The nature of comet-asteroid transition object (3200) Phaethon. *Astronomy & Astrophysics, 461*, 751–757.

Pieters, C. M., Hiroi, T. (2004). RELAB (Reflectance Experiment Laboratory): A NASA

multiuser spectroscopy facility. In: Mackwell, S., Stansbery, E. (Eds.), *Lunar Planet. Inst. Sci. Conf. Abstracts, 35,* 1720.

Pinilla-Alonso, N., Alvarez-Candal, A., Melita, M.D., Lorenzi, V., Licandro, J. Carvano, J. Lazzaro, D., Carraro, G., Ali-Lagoa, V., Costa, E., Hasselmannet P. H. (2013) Surface composition and dynamical evolution of two retrograde objects in the outer solar system: 2008 YB3 and 2005 VD. *Astronomy & Astrophysics, 550,* A13.

Popescu, M., Birlan, M., Nedelcu, D.A. (2012). Modeling of asteroid spectra – M4AST. *Astronomy & Astrophysics, 544,* A130.

Sawyer, S. (1998). Sawyer Asteroid Spectra. EAR-A-3-RDR-SAWYER-ASTEROID-SPECTRA-V1.2. NASA Planetary Data System.

Tholen, D.J. (1984). Asteroid Taxonomy from Cluster Analysis of Photometry. PhD thesis. AA Arizona Univ., Tucson.

Vilas, F. (1994), A cheaper, faster, better way to detect water of hydration on solar system bodies, *Icarus, 111*, 456–467.

Vilas, F., & Gaffey, M.J. (1989). Phyllosilicate absorption features in main-belt and outer-belt asteroid reflectance spectra. *Science, 246*, 790–792.

Wiegert, P., Balam, D., Moss, A.; Veillet, C., Connors, M., Shelton, I. (2007). Evidence for a Color Dependence in the Size Distribution of Main-Belt Asteroids. *The Astronomical Journal*, *133*, 1609–1614.

Zellner, B., Tholen, D.J., Tedesco, E.F. (2009). Eight Color Asteroid Survey. EAR-A-2CP-3-RDR-ECAS-V4.0. *NASA Planetary Data System.*